

UCLA

UCLA Previously Published Works

Title

Structure and substrate selectivity of the 750-kDa $\alpha\beta\delta$ holoenzyme of geranyl-CoA carboxylase

Permalink

<https://escholarship.org/uc/item/7db498d6>

Journal

Nature Communications, 6(1)

ISSN

2041-1723

Authors

Jurado, Ashley R
Huang, Christine S
Zhang, Xing
et al.

Publication Date

2015

DOI

10.1038/ncomms9986

Peer reviewed

ARTICLE

Received 28 Jun 2015 | Accepted 22 Oct 2015 | Published 23 Nov 2015

DOI: 10.1038/ncomms9986

OPEN

Structure and substrate selectivity of the 750-kDa $\alpha_6\beta_6$ holoenzyme of geranyl-CoA carboxylase

Ashley R. Jurado^{1,*}, Christine S. Huang^{1,*}, Xing Zhang², Z. Hong Zhou^{2,3} & Liang Tong¹

Geranyl-CoA carboxylase (GCC) is essential for the growth of *Pseudomonas* organisms with geranic acid as the sole carbon source. GCC has the same domain organization and shares strong sequence conservation with the related biotin-dependent carboxylases 3-methylcrotonyl-CoA carboxylase (MCC) and propionyl-CoA carboxylase (PCC). Here we report the crystal structure of the 750-kDa $\alpha_6\beta_6$ holoenzyme of GCC, which is similar to MCC but strikingly different from PCC. The structures provide evidence in support of two distinct lineages of biotin-dependent acyl-CoA carboxylases, one carboxylating the α carbon of a saturated organic acid and the other carboxylating the γ carbon of an α - β unsaturated acid. Structural differences in the active site region of GCC and MCC explain their distinct substrate preferences. Especially, a glycine residue in GCC is replaced by phenylalanine in MCC, which blocks access by the larger geranyl-CoA substrate. Mutation of this residue in the two enzymes can change their substrate preferences.

¹Department of Biological Sciences, Columbia University, New York, New York 10027, USA. ²California NanoSystems Institute, University of California, Los Angeles, California 90095, USA. ³Department of Microbiology, Immunology and Molecular Genetics, University of California, Los Angeles, California 90095, USA. *These authors contributed equally to this work. Correspondence and requests for materials should be addressed to L.T. (email: ltong@columbia.edu)

Terpenes are a common biosynthetic precursor of many biological compounds, including hormones and cholesterol, and have long been studied for their many medicinal properties^{1–3}. Monoterpenes are the simplest terpenes and are formed by the joining of two five-carbon isoprene units. Terpenes are modified and cyclized in various ways to form numerous terpenoids, including hormone precursors, scents, and flavourings. Isoprenylation is also used for localizing proteins to the cell membrane. In certain bacteria, terpenes can be used as the primary carbon source and metabolized to enter the tricarboxylic acid cycle as acetyl-CoA.

Geranyl-CoA carboxylase (GCC) activity was first purified from a *Pseudomonas* organism grown with either the related acyclic monoterpene citronellol⁴ or geranic acid^{5–7} as the sole carbon source. GCC also possesses 3-methylcrotonyl-CoA carboxylase (MCC) activity^{5,6,8}, and 3-methylcrotonyl-CoA is an intermediate in the complete catabolism of citronellol and geranic acid (Fig. 1a). In comparison, the authentic MCC enzyme cannot carboxylate the larger geranyl-CoA substrate. GCC and other enzymes involved in the first half of the geranic acid degradation pathway are encoded by the acyclic terpene utilization operon, while MCC and those involved in the second half are encoded by the leucine/isovalerate utilization operon^{8,9}. GCC is found in *Pseudomonas* and a collection of other bacteria. MCC is conserved from bacteria to humans, and is crucial for leucine metabolism (Fig. 1a). Deficiencies in MCC activity in humans are linked to methylcrotonylglycinuria and other serious metabolic diseases^{10–12}.

GCC and MCC are members of the biotin-dependent carboxylase superfamily^{13–17}. Both consist of two subunits, α and β , and their holoenzymes are 750-kDa- $\alpha_6\beta_6$ dodecamers. The α subunit contains the biotin carboxylase (BC), BC–CT interaction (BT)^{18,19}, and the biotin carboxyl carrier protein (BCCP) domains (Fig. 1b, Supplementary Fig. 1). The β subunit contains the N and C domains of carboxyltransferase (CT, Supplementary Fig. 2). The α subunits of *Pseudomonas* GCC and MCC share 51% amino acid sequence identity, and their

β subunits share 46% identity. These two enzymes therefore have high sequence conservation, but the molecular basis for their distinct substrate preferences is currently not known. In fact, many of the GCC/MCC enzymes in the sequence database have been misannotated (see below).

Propionyl-CoA carboxylase (PCC) shares the same domain organization as GCC and MCC (Fig. 1b). However, our recent crystal structures of MCC and PCC showed that their holoenzymes have strikingly different overall architectures^{18,19}. Moreover, the connectivity between the N and C domains is different in the two β subunits (Supplementary Fig. 3). These results led to the hypothesis that there are two distinct lineages of biotin-dependent acyl-CoA carboxylases¹⁹: those that carboxylate the α carbon of the organic acid (PCC, acetyl-CoA carboxylase) and those that carboxylate the γ carbon of an α - β unsaturated acid (MCC, GCC) (Fig. 1a). A prediction of this hypothesis is that GCC should have a similar β subunit connectivity as MCC, and that the GCC holoenzyme may have a similar architecture as MCC. Here we report the crystal structure of the GCC holoenzyme, as well as mutagenesis studies to define the molecular basis for the distinct substrate preferences of GCC and MCC.

Results

Structure of GCC β subunit hexamer. We first determined the structure of *Pseudomonas aeruginosa* GCC (PaGCC) β subunit at 2.4 Å resolution. The current atomic model has good agreement with the crystallographic data and the expected geometric parameters (Table 1). The structure confirms our hypothesis, showing that GCC β has the same connectivity between its N and C domains as that of MCC β (Fig. 2a). The overall structures of the two subunits are similar, with root mean squared distance of 1.2 Å for 464 equivalent C α atoms between them, consistent with their strong sequence conservation. The overall structures of the two β_6 hexamers are similar to each other as well, with root mean squared distance of 1.3 Å for 2,866 equivalent C α atoms (Fig. 2b).

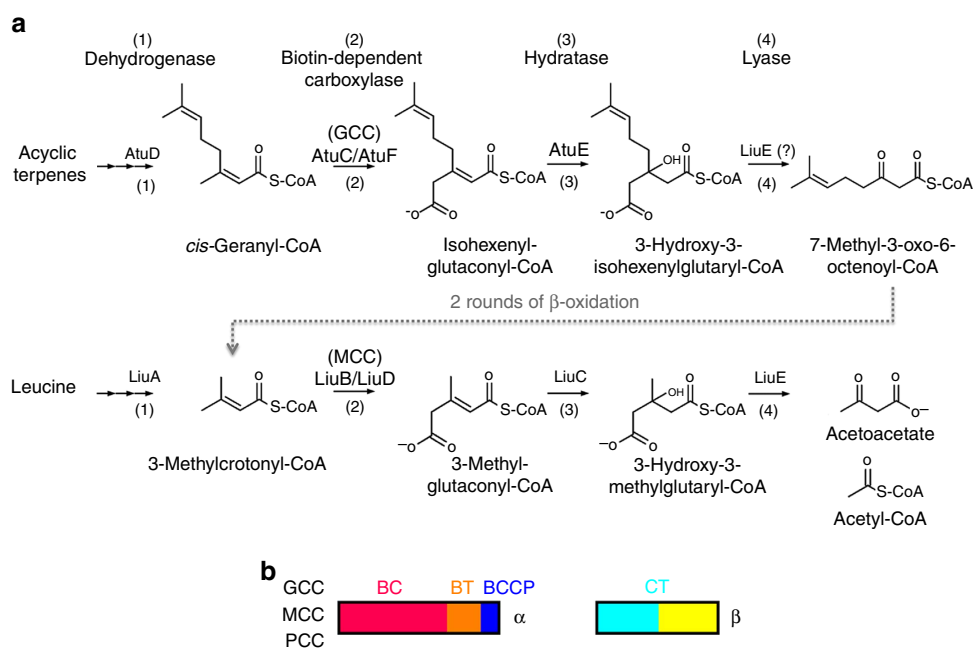


Figure 1 | The metabolic pathways involving GCC and MCC. (a) The metabolism of acyclic terpenes requires the activity of both GCC and MCC, while the metabolism of the amino acid leucine requires only MCC. The Atu and Liu pathways are sequentially similar, involving dehydrogenase, carboxylase, hydratase and lyase activities. (b) Domain organization of GCC, MCC and PCC α and β subunits. The various domains are labeled. Atu, acyclic terpene utilization; Liu, leucine/isovalerate utilization.

Table 1 | Summary of crystallographic information.

	PaGCC β hexamer	PfGCC holoenzyme
<i>Data collection</i>		
Space group	<i>P</i> 6 ₅ 22	<i>P</i> 4 ₁ 2 ₁ 2
Cell dimensions		
<i>a</i> , <i>b</i> , <i>c</i> (Å)	105.7, 105.7, 550.8	234.6, 234.6, 274.4
α , β , γ (°)	90, 90, 120	90, 90, 90
Resolution (Å)*	30–2.4 (2.53–2.4)	50–3.1 (3.26–3.1)
<i>R</i> _{merge}	8.4 (43.2)	12.2 (>100)
CC _{1/2}	–	0.48
<i>I</i> / σ <i>I</i>	15.4 (3.1)	9.7 (1.0)
Completeness (%)	100 (99)	98 (95)
Redundancy	4.5 (4.5)	3.7 (3.6)
<i>Refinement</i>		
Resolution (Å)	47–2.4	50–3.1
No. of reflections	68,848	128,390
<i>R</i> _{work} / <i>R</i> _{free}	21.6/26.2	19.6/22.8
No. of atoms		
Protein	11,411	25,281
Ligand/ion	0	0
Water	172	0
<i>B</i> -factors		
Protein	66	99
Ligand/ion	–	–
Water	52	–
R.m.s. deviations		
Bond lengths (Å)	0.013	0.011
Bond angles (°)	1.6	1.5

PaGCC, *Pseudomonas aeruginosa* geranyl-CoA carboxylase; PfGCC, *Pseudomonas fluorescens* geranyl-CoA carboxylase; r.m.s., root mean squared.
*The numbers in parentheses are for the highest resolution shell.

However, there are regions of substantial conformational differences between the two subunits. While the connectivity in GCC β is the same as in MCC β , the linker between the N and C domains has a different conformation (Fig. 2a). In addition, the C-terminal segment of GCC β (residues 526–538) contacts the N domain, while that of MCC β contacts the C domain. The long helix at the N-terminal end of GCC β is disordered in one of the three β subunits in the asymmetric unit (Fig. 2b), although this helix is fully ordered in the GCC holoenzyme structure. Finally, structural differences in the active site region of the two enzymes define their distinct substrate preferences (see below).

Structure of 750-kDa GCC holoenzyme. We next determined the crystal structure at 3.1 Å resolution of the *Pseudomonas fluorescens* (also known as *P. protegens*) GCC (PfGCC) holoenzyme (Table 1, Supplementary Fig. 4). The overall architecture of the GCC holoenzyme is similar to that of MCC (Fig. 3a), consistent with our hypothesis. The GCC α subunits are arranged as trimers above and below the GCC β_6 hexamer core (Fig. 3b), forming an elongated, cylinder-shaped holoenzyme structure (Fig. 3a). The height of the holoenzyme is \sim 200 Å and the diameter of the cylinder is \sim 100 Å. When the β_6 cores of GCC free enzyme and MCC holoenzyme in complex with CoA are superposed, the BC domain in each GCC α subunit shows \sim 9° difference in orientation compared with its equivalent in MCC (Fig. 3b). A similar difference is seen for the orientation and position of the BT domains in the two enzymes (Fig. 3a). In comparison, a difference of \sim 6° was observed for the α subunit between the MCC free enzyme and the CoA complex¹⁹, and the structure of GCC free enzyme is somewhat more similar to that of the MCC free enzyme, with a difference of \sim 4°. Therefore, there might be some inherent flexibility in the orientation of the α subunits relative to the β_6 core in these holoenzymes.

The distance between the BC and CT active sites is \sim 80 Å in the GCC holoenzyme (Fig. 3a). Therefore, the entire BCCP domain must translocate during GCC catalysis, as is the case with MCC (ref. 19), PCC (ref. 18), long-chain acyl-CoA carboxylase²⁰, pyruvate carboxylase^{21–24}, and urea carboxylase²⁵. The BCCP-biotin is bound in the active site of the CT domain in the current structure, at roughly the same position as that in the MCC holoenzyme (Fig. 3a). In four of the six BCCP domains in the GCC holoenzyme, a portion of the structure located farthest from the holoenzyme core is disordered. In comparison, only one of the six BCCP domains is ordered in the MCC holoenzyme (Fig. 3a)¹⁹.

We also carried out cryo electron microscopy (cryoEM) studies on the PfGCC holoenzyme and produced a reconstruction at 5.6 Å resolution (Fig. 4a,b). The crystal structure and the cryoEM reconstruction are in excellent agreement with each other overall. The cryoEM studies therefore provide important, independent confirmation that GCC assumes the same structure in solution. The four B subdomains of BC that are disordered in the crystal are observed by cryoEM. However, the two B subdomains observed in the crystal show a different conformation in the cryoEM reconstruction. The disordered segments of the BCCP domains in the crystal are also observed by cryoEM (Fig. 4a), but the overall positions of the BCCP domains in the CT active site are essentially the same in the crystal structure and cryoEM reconstruction.

A BT domain in the structure of GCC. The sequences of the BT domains are not well conserved among GCC, MCC and PCC, in contrast to the BC and CT domains (Supplementary Figs 1,2). The structure of the BT domain in GCC consists of a long α -helix (α V) surrounded by an eight-stranded anti-parallel β -barrel (β 22– β 29, Fig. 5a). In comparison, the helix of the MCC BT domain is shorter (Fig. 5b), and its β -barrel is missing a strand (β 24, Fig. 5a), although this might be unique to *P. aeruginosa* and closely related MCCs (Supplementary Fig. 1)¹⁹. In this regard, the structure of the GCC BT domain appears more similar to that of the PCC BT domain (Fig. 5c). On the other hand, the long loop connecting the helix to the first β strand, the ‘hook’¹⁸, has different conformations in the three BT domains, and mediates unique interactions that may help to determine the relative positions of the α and β subunits in these holoenzymes. These unique interactions also ensure the fidelity of each holoenzyme, such that a GCC-MCC hybrid cannot be produced.

The C-terminal segment of this hook in the GCC BT domain contains a short β -strand and establishes similar interactions with the β subunit as observed in MCC (Fig. 5a). The first residue of this β -strand is Trp483, mostly conserved among GCC and MCC enzymes (Trp543 in PaMCC, residue numbers according to human MCC, Supplementary Fig. 1). The side chain is buried at the interface between the N and C domains of the β subunit. This part of the hook is also located near the long helix (α 0) at the N-terminal end of the β unit, a structural feature that is absent in PCC.

The N-terminal segment of the hook in the MCC BT domain is much longer, and establishes interactions with the linker between the N and C domains of the β subunit (Fig. 5b). In fact, the conformational differences for this linker between GCC and MCC (Fig. 2a) are likely due to this interaction with the BT domain in MCC, as the conformation of the linker in the GCC holoenzyme would clash with this part of the hook in the MCC holoenzyme (Fig. 5b). This different conformation of the linker, by up to 10 Å, is in turn coupled to the different positioning of the C-terminal segments of the β subunits. The C-terminal segments of two monomers in a β_2 dimer are swapped with each other

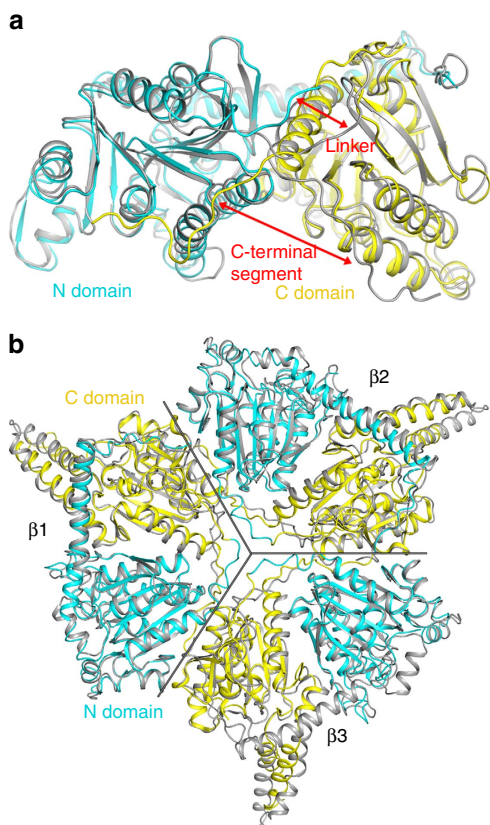


Figure 2 | The structure of GCC β subunit. (a). Overlay of the structure of PaGCC β subunit (in colour) with that of PaMCC β subunit (PDB entry 3U9R, in grey)¹⁹. Large conformational differences for the linker between the N and C domains and the C-terminal segment are indicated with the red arrows. (b). Overlay of the structure of PaGCC β subunit trimer (in colour) with that of PaMCC β subunit trimer (in grey). The subunit boundaries are indicated with the grey lines. The three β subunits in the bottom layer of the β_6 hexamer have been omitted for clarity. The long helix at the N terminus is missing in β_3 . All the structure figures were produced with PyMOL (www.pymol.org) unless stated otherwise.

between GCC and MCC (Fig. 5b), again illustrating the dramatic structural plasticity among these highly conserved enzymes.

Molecular basis for substrate preference. Based on the binding modes of CoA to MCC (ref. 19) and crotonyl-CoA to glutaconyl-CoA decarboxylase α (ref. 26), we built a model for the binding mode of geranyl-CoA in GCC (Fig. 6a). There is a large, mostly hydrophobic pocket at the bottom of the active site in GCC that can accommodate the larger geranyl group. The pocket is formed primarily by residues in helices α_3 , α_4 and α_5 in the N domain, with only minor contributions from residues in the C domain. Interestingly, the side chain of Phe191 in MCC β is located in this pocket and clashes with the second isopentenyl group of geranyl-CoA. The equivalent residue in GCC is Gly162. There are also differences in the main-chain atoms of the residues in this region, and MCC β contains a three-residue insertion here (Supplementary Fig. 2). Overall, these structural differences reduce the size of the active site pocket in MCC β , thereby defining the molecular basis for why MCC is not active toward the larger geranyl-CoA substrate. Conversely, the larger pocket in GCC can accommodate both geranyl-CoA and 3-methylcrotonyl-CoA, and therefore it can be active toward both substrates.

To test these structural observations, we created the G162F mutant of GCC β and the F191G mutant of MCC β . The G162F mutation destabilized the GCC holoenzyme and it dissociated during gel filtration unless stabilized by higher salt concentrations. The activity of wild-type GCC toward the geranyl-CoA substrate (Fig. 6b) is about fourfold lower than that of wild-type MCC toward the 3-methylcrotonyl-CoA substrate (Fig. 6c). Wild-type GCC showed very weak activity towards 3-methylcrotonyl-CoA. The K_m of this reaction is very high, suggesting that binding of the smaller CoA compound is not optimal in the GCC active site.

As predicted by the structure, the G162F mutant of GCC is catalytically inactive toward geranyl-CoA, while the F191G mutant of MCC showed appreciable activity towards this substrate, about fivefold lower than wild-type GCC (Fig. 6b). Conversely, the G162F mutant of GCC demonstrates stronger activity towards 3-methylcrotonyl-CoA than wild-type GCC, while the F191G mutant of MCC is essentially inactive (Fig. 6c).

Discussion

The kinetic parameters reported here for the wild-type enzymes are generally similar to those from previous studies on GCC and MCC. An apparent K_m value of 50 μ M was determined from our studies on PfGCC (Fig. 6b). However, only $\sim 25\%$ of the geranyl-CoA compound we used was in the *cis* configuration. Therefore, the actual K_m value is likely $\sim 12 \mu$ M, comparable to the 9 μ M reported earlier for PaGCC (ref. 8). The K_m value for PaMCC was 69 μ M based on our studies (Fig. 6c), while the earlier study reported 10 μ M as well as cooperative behaviour (Hill coefficient 2.3). However, in a more recent paper²⁷, the K_m was found to be 220 μ M and no cooperativity was reported. These other kinetic studies are based on the CO₂ fixation assay, while our studies are based on the coupled enzyme assay monitoring ATP hydrolysis. Some of the differences in the kinetic parameters could also be due to the differences in the assay protocols.

Since GCC, MCC, and PCC have similar domain organizations (Fig. 1b) and conserved sequences, we have found that they are frequently misannotated in the sequence database. The structural information on the three holoenzymes suggests guidelines for how they can be classified based on their sequences. PCC β lacks an extended α -helix (~ 30 residues) at the N terminus and can be separated from GCC β and MCC β based on this. The mitochondrial targeting sequence of animal PCC β should be excluded from this consideration. MCC β has a Phe residue in the active site region of the N domain, and this residue is replaced a Gly in GCC β . MCC β also has a short insertion of 3 residues just before this Phe residue compared with GCC β . With these guidelines, it should be possible to accurately annotate the different enzymes.

Overall, our studies on GCC, MCC and PCC support the presence of two distinct lineages of biotin-dependent acyl-CoA carboxylases. The structural differences among these enzymes also have wide implications for the relationship between sequence conservation and structural similarity. The differences in substrate preferences between GCC and MCC are defined by differences in their sequences, and consequently structures, in the active site region.

Methods

Protein expression and purification. GCC holoenzymes were overexpressed using a bi-cistronic plasmid, with GCC α (untagged) placed downstream of GCC β (N-terminal His-tagged) in a similar fashion to the MCC and PCC holoenzymes^{18,19}. The hexa-histidine tag was not removed for crystallization.

PaGCC holoenzyme was overexpressed in *Escherichia coli* BL21 Star (DE3) cells (Novagen) in the presence of 1 mM IPTG (Gold Biotechnology, Inc) to induce expression and incubated at 20 $^{\circ}$ C overnight. The soluble protein was eluted from Ni-NTA beads (Qiagen) and further purified by gel filtration in a column buffer

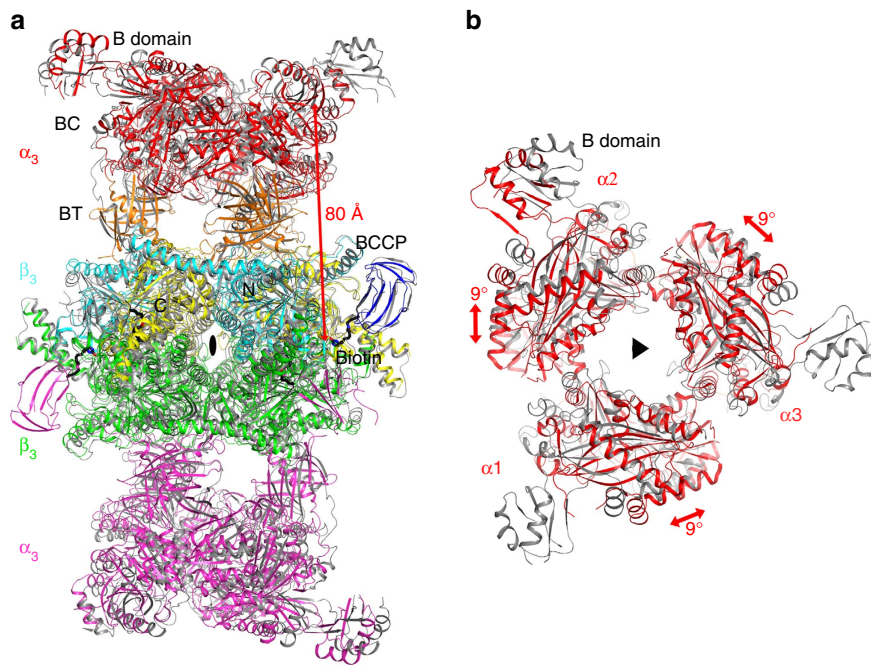


Figure 3 | The crystal structure of the GCC holoenzyme. (a). Overlay of the structure of PfgGCC holoenzyme (in colour) with that of PaMCC holoenzyme (PDB entry 3U9T, in grey)¹⁹, viewed down the two-fold symmetry axis of a β_2 dimer (black oval). Domains in the α and β subunits in the top half of the structure are coloured as in Fig. 1b for GCC. The α and β subunits in the bottom half are coloured in magenta and green, respectively. (b). Overlay of the structure of three BC domains in PfgGCC (in red) with that of the BC domains in PaMCC (in grey), viewed down the three-fold symmetry axis of the holoenzyme (black triangle). The differences in the conformations of the BC domains are indicated with the red arrows, corresponding to a rotation of $\sim 9^\circ$. Only one of the B domains of BC in the $\alpha_3\beta_3$ asymmetric unit is ordered in PfgGCC.

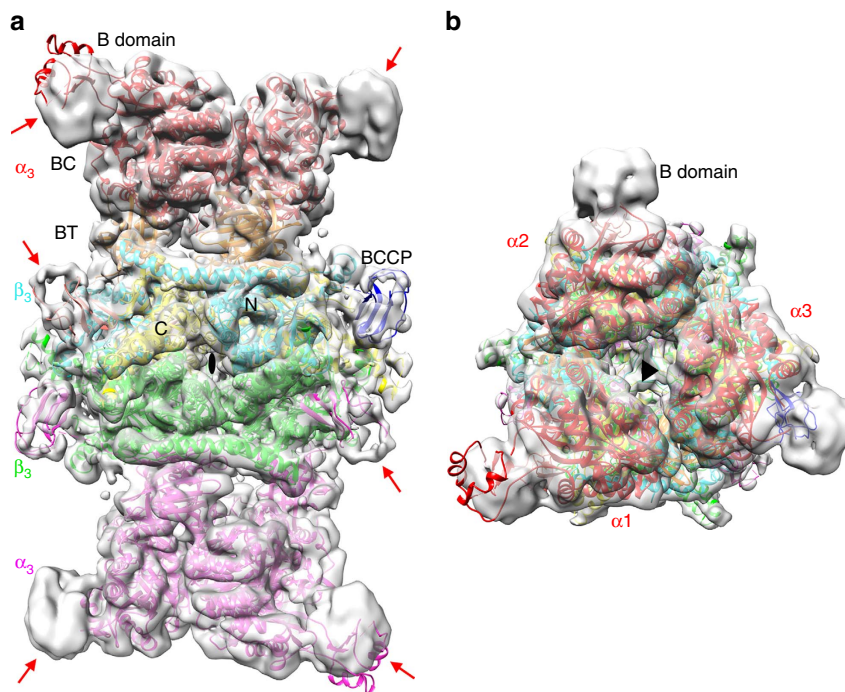


Figure 4 | The cryo electron microscopy structure of the GCC holoenzyme. (a). CryoEM reconstruction of PfgGCC at 5.6 Å resolution, shown as a transparent surface (in grey) and viewed in the same orientation as Fig. 3a. The crystal structure of PfgGCC can be readily fit into the cryo EM density. Several of the B domains of BC and the disordered segments of BCCP in the crystal structure are observed in the cryo EM density, indicated with the red arrows. The conformation of the two ordered B domains in the crystal is somewhat different from that observed by EM. (b). Cryo EM reconstruction of PfgGCC, viewed down the three-fold symmetry axis of the holoenzyme (black triangle). Produced with Chimera³⁸.

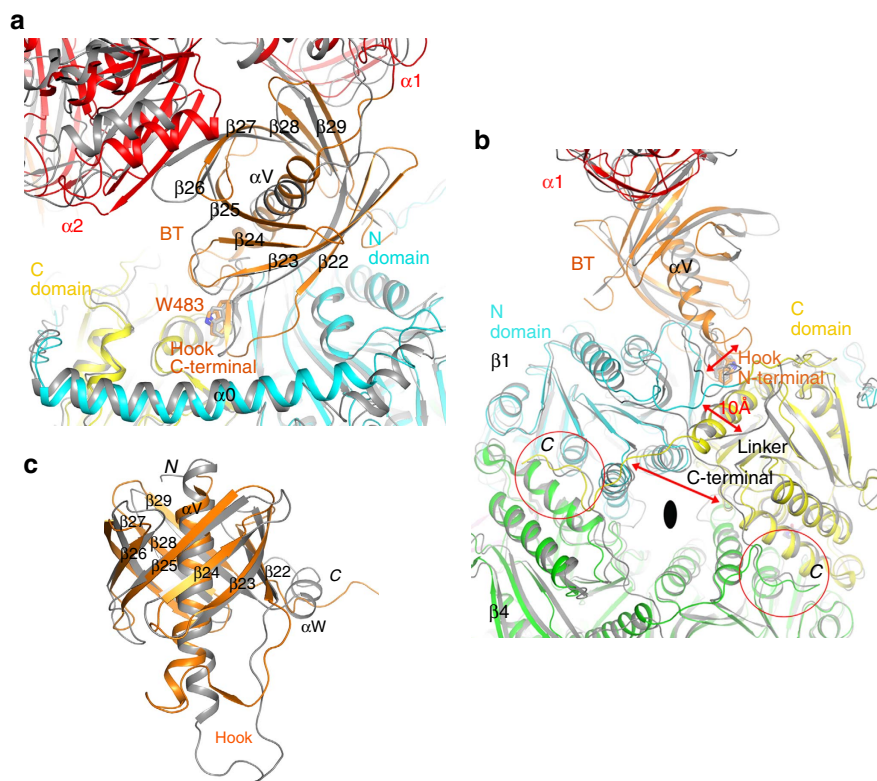


Figure 5 | Interactions between the BT domain and the β subunit in the GCC holoenzyme. (a). Comparison of the interactions between the C-terminal segment of the hook in the BT domain and the β subunit in PfgGCC (in colour) with those in PaMCC (in grey). Strand $\beta 24$ is missing in the PaMCC BT domain, and the exact positions of many of the other β strands in the two BT domains are different as well. (b). Comparison of the interactions between the N-terminal segment of the hook in the BT domain and the β subunit in PfgGCC (in colour) with those in PaMCC (in grey). Large conformational differences are indicated with the red arrows and labelled. The C termini of the β subunits are highlighted with the red circles. The C-terminal segments of the β_2 dimer are swapped in GCC compared with MCC. (c). Overlay of the structure of GCC BT domain (in orange) with that of PCC (grey). A large conformational difference for the hook is visible.

containing 25 mM Tris (pH 7.4), 250 mM NaCl and 2 mM DTT. The purified protein was concentrated to 12 mg ml⁻¹, supplemented with 5% (v/v) glycerol, flash-frozen with liquid nitrogen and stored at -80 °C. An SDS gel of this sample showed that the α subunit was present in significantly substoichiometric amounts.

P. fluorescens GCC (PfgGCC) holoenzyme was expressed in the same condition as the PaGCC holoenzyme and purified by gel filtration in a column buffer containing 20 mM Tris (pH 8.5), 200 mM NaCl and 10 mM DTT. The purified protein was concentrated to 20 mg ml⁻¹, supplemented with 5% (v/v) glycerol, flash-frozen with liquid nitrogen and stored at -80 °C. An SDS gel of this sample showed stoichiometric amounts of both subunits.

Protein crystallization. Crystals of PaGCC β_6 hexamer were obtained by using the PaGCC holoenzyme protein sample (but with significantly substoichiometric amounts of the α subunit) with the hanging-drop vapour diffusion method. Crystals of PaGCC β subunit appeared after 2 weeks at 20 °C from a precipitant solution containing 100 mM Tris (pH 8.0) and 60% (v/v) MPD. Crystals were flash-frozen in liquid nitrogen for data collection at 100 K. Interestingly, crystals obtained by using a pure PaGCC β_6 sample diffracted very poorly.

Crystals of the PfgGCC holoenzyme were obtained using the microbatch-under-oil method at 20 °C. The protein (20 mg ml⁻¹) was mixed with the precipitant solution at a ratio of 2:1, which contained 100 mM Tris (pH 7.0), 2 M (NH₄)₂SO₄ and 250 mM Li₂SO₄. Crystals appeared after 1 month, and were cryoprotected by supplementing the precipitant solution with 30% (v/v) ethylene glycol.

Data collection and structure determination. X-ray diffraction data sets were collected on an ADSC Q315 CCD at the X29A beamline and on a Pilatus 6 M detector at the X25 beamline of the National Synchrotron Light Source at the Brookhaven National Laboratory. The diffraction images were processed using the HKL package²⁸. The data processing and refinement statistics are summarized in Table 1. The resolution limit for the PfgGCC holoenzyme data was determined using the CC_{1/2} criterion²⁹.

Crystals of PaGCC β contained one β_3 trimer in the asymmetric unit. The structure was determined by the molecular replacement method with the program Phaser³⁰, using the structure of MCC β as the model¹⁹. Crystals of the PfgGCC

holoenzyme contained half of the dodecamer ($\alpha_3\beta_3$) in the asymmetric unit. The structure was determined with the molecular replacement method using GCC β_3 and MCC α_3 as the search models. Structure refinement was carried out with the programs CNS³¹ and Refmac³², and the program Coot³³ was used for manual model rebuilding.

CryoEM imaging. To prepare cryoEM grids, we applied 2 μ l of purified PfgGCC sample to thin continuous carbon films on lacey grids (Ted Pella Inc.) for 1 min, blotted for 12 s under 100% humidity and plunged the grid into liquid ethane with an FEI Vitrobot (ambient temperature in the Vitrobot chamber was 20 °C). CryoEM images were collected at liquid nitrogen temperature in an FEI Titan Krios cryo electron microscope operated at 300 kV using parallel illumination. Before data collection, the microscope was carefully aligned, and beam tilt was minimized by coma-free alignment. Images were recorded on a Gatan K2 camera with the counting mode at a nominal magnification of $\times 29,000$ on microscope. The magnification on the camera was calibrated as $\times 49,500$ using a catalase crystal sample, giving a pixel size of 1.01 Å per pixel on specimen. The dose rate of the electron beam was set to ~ 8 counts per pixel per s on the camera which corresponds to $\sim 10 e^- \text{Å}^{-2} \text{s}^{-1}$ on specimen when including the electrons uncounted by the K2 camera. Image stacks were recorded at 4 frames per sec for 10 s. After drift correction with the UCSF software³⁴, the first 12 frames of each image stack (movie) were merged to generate a final image with a total dose of $\sim 30 e^- \text{Å}^{-2}$ of the sample.

CryoEM image processing. A total of 41,271 particle images were picked from 1,149 images automatically with the *Dog Picker* program³⁵. The under defocus values of these images were determined to be between 1.06 to 3.4 μ m using CTFFIND³⁶. Image processing and reconstruction were carried out using RELION³⁷. Two-dimensional classification was first used to screen particles. After 25 iterations, 16 two-dimensional classes with 31,206 particles were picked from the total 30 classes. Three-dimensional (3D) classification was then performed with RELION to classify all particles into three groups. However, the reconstructions from these three groups are nearly identical. We therefore used all 31,206 particles for 3D refinement, which started from a featureless starting model generated by

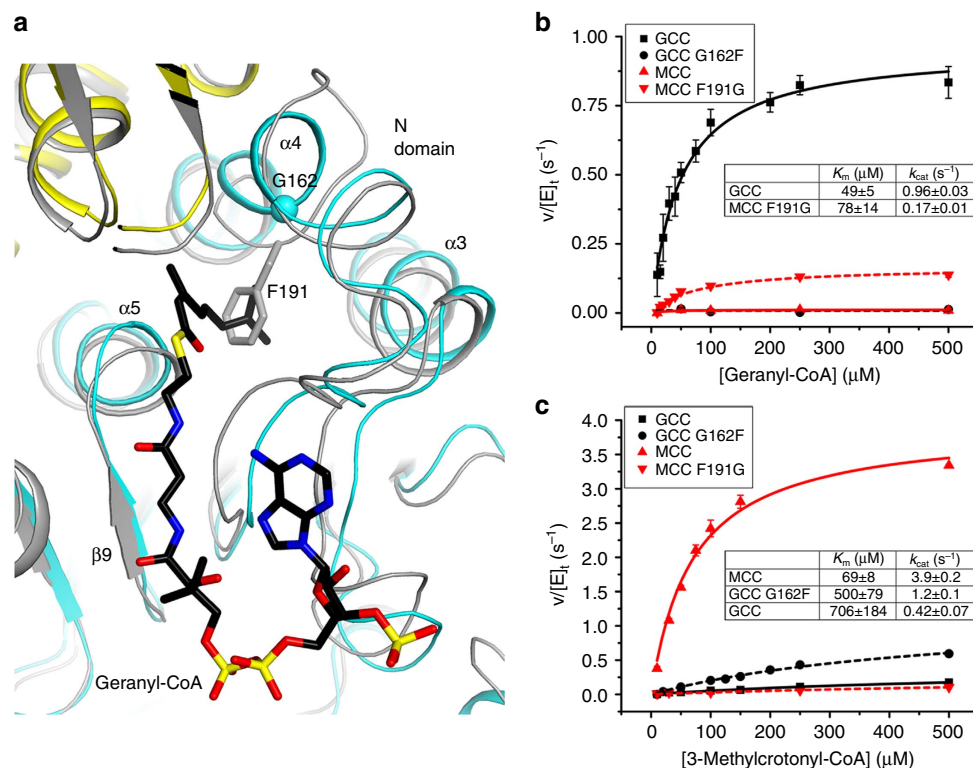


Figure 6 | Molecular basis for the different substrate preferences of GCC and MCC. (a) A model for the binding mode of the geranyl-CoA substrate (in black) in the active site of GCC (cyan for the N domain and yellow for the C domain of the β subunits). The structure of MCC is superimposed and shown in grey. The side chain of Phe191 of MCC β is shown as a stick model (grey), and the C_α atom of Gly162 of GCC β is shown as a sphere (cyan). (b) Catalytic activities of wild-type GCC and MCC, the G162F mutant of GCC and the F191G mutant of MCC toward the geranyl-CoA substrate. The error bars represent the standard deviations from three separate experiments. The kinetic parameters are shown in the inset. (c). Catalytic activities of wild-type GCC and MCC, the G162F mutant of GCC and the F191G mutant of MCC toward the 3-methylcrotonyl-CoA substrate.

low-pass (60 Å resolution) filtering the structure of MCC (PDB code: 3U9T; ref. 19). The 32 symmetry of the particles was also applied in the calculation. After 16 cycles of 3D refinement, the resolution of GCC structure was estimated to be ~ 5.6 Å using the ‘gold-standard FSC’ criterion with RELION. The density map was sharpened with a reverse B-factor of -250 Å². Visualization and segmentation of density maps were carried out with UCSF Chimera³⁸.

Mutagenesis and kinetic studies. Site-specific mutations in PfGCC and PaMCC were introduced with the QuikChange kit (Agilent Technologies) and expressed and purified under the same conditions as PfGCC (gel filtration buffer 20 mM Tris (pH 8.5), 200 mM NaCl, 5 mM DTT).

The catalytic activity of PaMCC, PfGCC and their mutants was determined using a coupled enzyme assay, converting the hydrolysis of ATP to the disappearance of NADH (refs 39,40). The reaction mixture contained 100 mM HEPES (pH 8.0), 0.5 mM ATP, 8 mM MgCl₂, 40 mM KHCO₃, 2–500 μM 3-methylcrotonyl-CoA or crotonyl-CoA, 0.2 mM NADH, 0.5 mM phosphoenolpyruvate, 7 units of lactate dehydrogenase, 4.2 units of pyruvate kinase and 250 mM KCl. The absorbance at 340 nm was monitored for 5 min. Geranyl-CoA was synthesized chemically from geranic acid and CoA (Changchun Discovery Sciences, Ltd), and contained $\sim 25\%$ *cis* isomer based on HPLC and proton NMR measurements. Based on the structure, the *trans* isomer is unlikely to be accommodated in the active site, and therefore could not serve as a substrate or an inhibitor of the enzyme.

References

- Thulasiram, H. V., Erickson, H. K. & Poulter, C. D. Chimeras of two isoprenoid synthases catalyze all four coupling reactions in isoprenoid biosynthesis. *Science* **316**, 73–76 (2007).
- Vranova, E., Coman, D. & Gruisern, W. Network analysis of the MVA and MEP pathways for isoprenoid synthesis. *Annu. Rev. Plant Biol.* **64**, 665–700 (2013).
- Rodriguez-Concepcion, M. Plant isoprenoids: a general overview. *Methods Mol. Biol.* **1153**, 1–5 (2014).
- Seubert, W., Fass, E. & Remberger, U. Studies on the bacterial degradation of isoprenoid compounds. III. Purification and properties of geranyl carboxylase. *Biochem. Z.* **338**, 265–275 (1963).
- Hector, M. L. & Fall, R. R. Multiple acyl-coenzyme A carboxylases in *Pseudomonas citronellolis*. *Biochemistry* **15**, 3465–3472 (1976).
- Hector, M. L. & Fall, R. R. Evidence for distinct 3-methylcrotonyl-CoA and geranyl-CoA carboxylases in *Pseudomonas citronellolis*. *Biochem. Biophys. Res. Commun.* **71**, 746–753 (1976).
- Fall, R. R. & Hector, M. L. Acyl-coenzyme A carboxylases. Homologous 3-methylcrotonyl-CoA and geranyl-CoA carboxylase from *Pseudomonas citronellolis*. *Biochemistry* **16**, 4000–4005 (1977).
- Aguilar, J. A. *et al.* Substrate specificity of the 3-methylcrotonyl coenzyme A (CoA) and geranyl-CoA carboxylases from *Pseudomonas aeruginosa*. *J. Bacteriol.* **190**, 4888–4893 (2008).
- Forster-Fromme, K. & Jendrossek, D. Catabolism of citronellol and related acyclic terpenoids in pseudomonads. *Appl. Microbiol. Biotechnol.* **87**, 859–869 (2010).
- Baumgartner, M. R. *et al.* The molecular basis of human 3-methylcrotonyl-CoA carboxylase deficiency. *J. Clin. Invest.* **107**, 495–504 (2001).
- Gallardo, M. E. *et al.* The molecular basis of 3-methylcrotonylglycinuria, a disorder of leucine metabolism. *Am. J. Hum. Genet.* **68**, 334–346 (2001).
- Holzinger, A. *et al.* Cloning of the human MCCA and MCCB genes and mutations therein reveal the molecular cause of 3-methylcrotonyl-CoA carboxylase deficiency. *Hum. Mol. Genet.* **10**, 1299–1306 (2001).
- Wakil, S. J., Stoops, J. K. & Joshi, V. C. Fatty acid synthesis and its regulation. *Annu. Rev. Biochem.* **52**, 537–579 (1983).
- Tong, L. Structure and function of biotin-dependent carboxylases. *Cell. Mol. Life Sci.* **70**, 863–891 (2013).
- Cronan, Jr. J. E. & Waldrop, G. L. Multi-subunit acetyl-CoA carboxylases. *Prog. Lipid Res.* **41**, 407–435 (2002).
- Jitrapakdee, S. *et al.* Structure, mechanism and regulation of pyruvate carboxylase. *Biochem. J.* **413**, 369–387 (2008).
- Nikolau, B. J., Ohlrogge, J. B. & Wurtele, E. S. Plant biotin-containing carboxylases. *Arch. Biochem. Biophys.* **414**, 211–222 (2003).
- Huang, C. S. *et al.* Crystal structure of the a6b6 holoenzyme of propionyl-coenzyme A carboxylase. *Nature* **466**, 1001–1005 (2010).
- Huang, C. S., Ge, P., Zhou, Z. H. & Tong, L. An unanticipated architecture of the 750-kDa a6b6 holoenzyme of 3-methylcrotonyl-CoA carboxylase. *Nature* **481**, 219–223 (2012).

20. Tran, T. H. *et al.* Structure and function of a single-chain, multi-domain long-chain acyl-CoA carboxylase. *Nature* **518**, 120–124 (2015).
21. St. Maurice, M. *et al.* Domain architecture of pyruvate carboxylase, a biotin-dependent multifunctional enzyme. *Science* **317**, 1076–1079 (2007).
22. Xiang, S. & Tong, L. Crystal structures of human and *Staphylococcus aureus* pyruvate carboxylase and molecular insights into the carboxyltransfer reaction. *Nat. Struct. Mol. Biol.* **15**, 295–302 (2008).
23. Yu, L. P. C. *et al.* A symmetrical tetramer for *S. aureus* pyruvate carboxylase in complex with coenzyme A. *Structure* **17**, 823–832 (2009).
24. Lasso, G. *et al.* Functional conformations for pyruvate carboxylase during catalysis explored by cryoEM. *Structure* **22**, 911–922 (2014).
25. Fan, C., Chou, C.-Y., Tong, L. & Xiang, S. Crystal structure of urea carboxylase provides insights into the carboxyltransfer reaction. *J. Biol. Chem.* **287**, 9389–9398 (2012).
26. Kress, D. *et al.* An asymmetric model for Na⁺-translocating glutacoyl-CoA decarboxylase. *J. Biol. Chem.* **284**, 28401–28409 (2009).
27. Diaz-Perez, C., Diaz-Perez, A. L., Rodriguez-Zavala, J. S. & Campos-Garcia, J. Structural evidence for the involvement of the residues Ser187 and Tyr422 in substrate recognition in the 3-methylcrotonyl-coenzyme A carboxylase from *Pseudomonas aeruginosa*. *J. Biochem.* **154**, 291–297 (2013).
28. Otwinowski, Z. & Minor, W. Processing of X-ray diffraction data collected in oscillation mode. *Method Enzymol.* **276**, 307–326 (1997).
29. Karplus, P. A. & Diederichs, K. Linking crystallographic model and data quality. *Science* **336**, 1030–1033 (2012).
30. McCoy, A. J. *et al.* Phaser crystallographic software. *J. Appl. Cryst.* **40**, 658–674 (2007).
31. Brunger, A. T. *et al.* Crystallography & NMR System: a new software suite for macromolecular structure determination. *Acta Crystallogr. D Biol. Crystallogr.* **54**, 905–921 (1998).
32. Murshudov, G. N., Vagin, A. A. & Dodson, E. J. Refinement of macromolecular structures by the maximum-likelihood method. *Acta Crystallogr. D Biol. Crystallogr.* **53**, 240–255 (1997).
33. Emsley, P. & Cowtan, K. D. Coot: model-building tools for molecular graphics. *Acta Crystallogr. D Biol. Crystallogr.* **60**, 2126–2132 (2004).
34. Li, X. *et al.* Electron counting and beam-induced motion correction enable near-atomic-resolution single-particle cryo-EM. *Nat. Methods* **10**, 584–590 (2013).
35. Voss, N., Yoshioka, C., Radermacher, M., Potter, C. & Carragher, B. DoG Picker and TiltPicker: software tools to facilitate particle selection in single particle electron microscopy. *J. Struct. Biol.* **166**, 205–213 (2009).
36. Mindell, J. A. & Grigorieff, N. Accurate determination of local defocus and specimen tilt in electron microscopy. *J. Struct. Biol.* **142**, 334–347 (2003).
37. Scheres, S. H. RELION: implementation of a Bayesian approach to cryo-EM structure determination. *J. Struct. Biol.* **180**, 519–530 (2012).
38. Pettersen, E. F. *et al.* UCSF Chimera—a visualization system for exploratory research and analysis. *J. Comput. Chem.* **25**, 1605–1612 (2004).
39. Diacovich, L. *et al.* Crystal structure of the b-subunit of acyl-CoA carboxylase: structure-based engineering of substrate specificity. *Biochemistry* **43**, 14027–14036 (2004).
40. Blanchard, C. Z., Lee, Y. M., Frantom, P. A. & Waldrop, G. L. Mutations at four active site residues of biotin carboxylase abolish substrate-induced synergism by biotin. *Biochemistry* **38**, 3393–3400 (1999).

Acknowledgements

We thank Neil Whalen and Stuart Myers for setting up the X29A beamline at the National Synchrotron Light Source. The in-house X-ray diffraction instrument was purchased with an NIH grant to LT (S10OD012018). This research was supported in part by NIH grants DK067238 (to LT) and GM071940 (to ZHZ). ARJ was also supported by an NIH training program in Cellular and Molecular Foundations of Biomedical Science (GM008798), and CSH was also supported by an NIH training program in molecular biophysics (GM008281). We acknowledge the use of electron microscopes at the Electron Imaging Center for Nanomachines supported by UCLA and by instrumentation grants from NIH (1S10RR23057, 1S10OD018111) and NSF (DBI-1338135).

Author contributions

A.R.J. and C.S.H. expressed, purified and crystallized the proteins. A.R.J., C.S.H. and L.T. determined the structures. A.R.J. carried out the mutagenesis and kinetic assays. X.Z. and Z.H.Z. carried out the cryoEM studies. Z.H.Z. and L.T. supervised the project, analyzed the data, and wrote the manuscript. All other authors commented on the manuscript.

Additional information

Supplementary Information accompanies this paper at <http://www.nature.com/naturecommunications>

Competing financial interests: The authors declare no competing financial interests.

Reprints and permission information is available online at <http://npg.nature.com/reprintsandpermissions/>

How to cite this article: Jurado, A. R. *et al.* Structure and substrate selectivity of the 750-kDa $\alpha_6\beta_6$ holoenzyme of geranyl-CoA carboxylase. *Nat. Commun.* **6**:8986 doi: 10.1038/ncomms9986 (2015).



This work is licensed under a Creative Commons Attribution 4.0 International License. The images or other third party material in this article are included in the article's Creative Commons license, unless indicated otherwise in the credit line; if the material is not included under the Creative Commons license, users will need to obtain permission from the license holder to reproduce the material. To view a copy of this license, visit <http://creativecommons.org/licenses/by/4.0/>